Research Square

Preprints are preliminary reports that have not undergone peer review.
They should not be considered conclusive, used to inform clinical practice,
or referenced by the media as validated information.

A Registration-consistent longitudinal CBCT framework for quantifying treatment- induced tumour morphology in head and neck radiotherapy

Karpaviciene Greta
Lithuanian University of Health Sciences
Meilutyte-Lukauskiene Diana
diana.meilutyte-lukauskiene@lei.lt

Lithuanian University of Health Sciences
Cerapaite-Trusinskiene Reda
Lithuanian University of Health Sciences
Paukstaitiene Renata
Lithuanian University of Health Sciences
Speckauskiene Vita
Lithuanian University of Health Sciences
Petrolis Robertas
Lithuanian University of Health Sciences

Research Article

Keywords: cone-beam CT, longitudinal imaging analysis, head and neck cancer, mixed-effects modelling, tumour heterogeneity, delta radiomics

Posted Date: June 8th, 2026

DOI: https://doi.org/10.21203/rs.3.rs-9664622/v1

License: This work is licensed under a Creative Commons Attribution 4.0 International License.
Read Full License

Additional Declarations: No competing interests reported.

A Registration-consistent longitudinal CBCT framework for quantifying treatment-induced tumour morphology in head and neck radiotherapy

Karpaviciene Greta[1,2], Meilutyte-Lukauskiene Diana[1,3*], Cerapaite-Trusinskiene Reda[1,2], Paukstaitiene Renata[1], Speckauskiene Vita[1], Petrolis Robertas[1,4]

[1]Department of Physics, Mathematics and Biophysics, Lithuanian University of Health Sciences, LT-44307 Kaunas, Lithuania
[2]Lithuanian University of Health Sciences Kaunas Clinics, Affiliated Hospital of Oncology, LT-45434 Kaunas, Lithuania
[3]Laboratory of Hydrology, Lithuanian Energy Institute, LT-44403 Kaunas, Lithuania
[4]Neuroscience Institute, Lithuanian University of Health Sciences, LT-50009 Kaunas, Lithuania.

**Corresponding author: D. Meilutyte-Lukauskiene. Email: diana.meilutyte-lukauskiene@lei.lt*

A Registration-consistent longitudinal CBCT framework for quantifying treatment-induced tumour morphology in head and neck radiotherapy

Karpaviciene Greta[1,2], Meilutyte-Lukauskiene Diana[1,3*], Cerapaite-Trusinskiene Reda[1,2], Paukstaitiene Renata[1], Speckauskiene Vita[1], Petrolis Robertas[1,4]

[1]Department of Physics, Mathematics and Biophysics, Lithuanian University of Health Sciences, LT-44307 Kaunas, Lithuania
[2]Lithuanian University of Health Sciences Kaunas Clinics, Affiliated Hospital of Oncology, LT-45434 Kaunas, Lithuania
[3]Laboratory of Hydrology, Lithuanian Energy Institute, LT-44403 Kaunas, Lithuania
[4]Neuroscience Institute, Lithuanian University of Health Sciences, LT-50009 Kaunas, Lithuania.

**Corresponding author: D. Meilutyte-Lukauskiene. Email: diana.meilutyte-lukauskiene@lei.lt*

Abstract

Background
Head and neck squamous cell carcinoma (HNSCC) exhibits substantial inter-patient variability in treatment response. Cone-beam computed tomography (CBCT) is routinely acquired during radiotherapy but remains underutilised for longitudinal tumour characterisation. This study aimed to develop a registration-consistent longitudinal CBCT framework for quantifying treatment-induced tumour morphology and to evaluate the temporal stability of radiomic features as candidate imaging biomarkers.

Methods
Thirty patients with HNSCC treated with definitive radiotherapy were retrospectively analysed. Tumour volumes defined on planning CT were propagated to daily CBCT images using rigid point-cloud registration to ensure spatial correspondence across treatment fractions. Radiomic features (entropy, strength, coarseness) were extracted within longitudinally aligned volumes of interest. Temporal dynamics were modelled using linear mixed-effects models incorporating treatment fraction, quadratic temporal terms, and tumour differentiation group (G1–G3).

Results
Entropy showed significant nonlinear temporal behaviour ($p < 0.001$), characterised by a mid-treatment peak and substantial inter-patient variability. Strength exhibited modest nonlinear variation without significant group-dependent effects. Coarseness demonstrated the most consistent longitudinal behaviour, with significant group-dependent temporal patterns ($p < 0.01$) and well-defined turning points across differentiation groups. Coarseness trajectories were less affected by high-frequency variation than entropy or strength.

Conclusion
Longitudinal CBCT-derived radiomic features capture dynamic tumour changes during radiotherapy, but their robustness varies substantially. Coarseness emerged as the most stable and interpretable feature, supporting a hierarchical interpretation in which coarseness may serve as a primary descriptor of treatment-induced structural change. The proposed framework provides a methodological basis for developing CBCT-based imaging biomarkers for longitudinal treatment monitoring and adaptive radiotherapy.

Keywords: cone-beam CT; longitudinal imaging analysis; head and neck cancer; mixed-effects modelling; tumour heterogeneity; delta radiomics

1 Introduction

Head and neck cancer (HNC) comprises a heterogeneous group of malignancies characterised by substantial variability in biological behaviour, treatment response, and clinical outcome. Radiotherapy remains a central component of HNC management, delivered as either a definitive or adjuvant modality, often in combination with systemic therapy [1]. Despite advances in treatment delivery, including intensity-modulated radiotherapy and image-guided techniques, clinical outcomes remain variable across patients, reflecting complex interactions among tumour biology, treatment sensitivity, and anatomical changes during therapy [2], [3]. This variability is further demonstrated by significant inter-patient differences in tumour regression dynamics during treatment [4], [5], [6].

During radiotherapy, substantial anatomical and structural changes occur, including tumour shrinkage, nodal regression, weight loss, and soft-tissue redistribution. These changes may lead to discrepancies between planned and delivered dose distributions, potentially resulting in underdosage of tumour regions or unintended exposure of organs at risk [5]. Adaptive radiotherapy (ART) has been proposed to account for such temporal changes by modifying treatment plans during therapy. Early evidence suggests that ART can improve dosimetric accuracy and maintain disease control [4]. However, despite these advantages, routine implementation remains limited due to increased workflow complexity and the lack of robust criteria for identifying patients who would benefit most from adaptation [6].

Cone-beam computed tomography (CBCT) is routinely acquired during radiotherapy for patient positioning and image guidance. In addition to geometric verification, CBCT provides volumetric anatomical information throughout the treatment course without additional imaging burden. However, in current clinical practise, CBCT is primarily used for quantitative or geometric assessment, while its potential for computational longitudinal analysis of tumour morphology remains underexplored. Importantly, CBCT images contain voxel-level intensity information reflecting treatment-induced changes, including oedema, necrosis, vascular alteration, and structural reorganisation [7].

Radiomics enables the extraction of quantitative image features that characterise intensity distributions and spatial heterogeneity within tumours. These features have been associated with tumour biology, treatment response, and clinical outcomes [8]. In head and neck oncology, increasing attention has been given to delta radiomics, which focuses on temporal changes in image-derived features during treatment [9], [10]. Compared with single-time-point analysis, longitudinal radiomic approaches offer the potential to capture continuous tumour evolution during therapy.

Despite this potential, several challenges limit the translation of CBCT-based radiomics into robust clinical biomarkers. CBCT images are affected by scatter, noise, and calibration variability, which complicate direct comparison of intensity values across time points [11]. Radiomic features are sensitive to image acquisition, preprocessing, segmentation, and feature extraction choices, leading to variability and limited reproducibility [12], [13]. Additional sources of uncertainty include heterogeneity in imaging parameters [14], variability in image registration strategies [15], and incomplete longitudinal datasets [16]. Furthermore, many existing studies rely on volumetric changes or pre- and post-treatment comparisons, rather than continuous modelling of feature dynamics within spatially consistent tumour regions.

A critical unmet need is therefore not only the extraction of longitudinal radiomic features, but also the identification of features whose temporal behaviour remains interpretable and stable under routine CBCT imaging conditions. Addressing this challenge requires methodological strategies that ensure spatial correspondence across time, mitigate CBCT-specific variability, and enable consistent within-patient analysis of voxel-level information. In addition, tumour differentiation is an established prognostic factor in head and neck cancer and may influence treatment response dynamics, its relationship with longitudinal imaging features remains insufficiently characterized [17].

In this study, we propose a registration-consistent longitudinal CBCT framework for quantifying treatment-induced tumour morphology during head and neck radiotherapy. The proposed approach combines baseline-defined tumour volume propagation, rigid point-cloud registration to ensure spatial alignment across treatment fractions, soft-tissue-constrained intensity analysis to reduce CBCT-related variability, and mixed-effects modelling of nonlinear temporal feature trajectories. Using this framework, we systematically evaluate the longitudinal behaviour of selected radiomic features and investigate their dependence on tumour differentiation. The goal of this work is to identify robust and interpretable imaging descriptors and provide a methodological basis for developing CBCT-based biomarkers for longitudinal treatment monitoring and adaptive radiotherapy.

2 Methods

2.1 Patient Cohort and Study Design

This retrospective study included 30 patients with histologically confirmed head and neck squamous cell carcinoma (HNSCC) treated with definitive concurrent radiotherapy at the Lithuanian University of Health Sciences Kaunas Clinics, Affiliated Hospital of Oncology, between January 2021 and December 2025. The study protocol was approved by the Kaunas Regional Biomedical Research Ethics Committee (No. BE-2-144), and all data were anonymised before analysis. The requirement for individual patient consent was waived due to the retrospective nature of the study and the use of fully anonymised data.

Patients were stratified by histological differentiation into three groups: well-differentiated (G1), moderately differentiated (G2), and poorly differentiated (G3), with 10 patients in each group. This balanced stratification enabled comparative longitudinal analysis of feature dynamics across differentiation grades.

The cohort included 22 (73.3%) male and 8 (26.7%) female patients (age range: 44–79 years). Tumour stages were distributed as follow: T1 (n = 3), T2 (n = 6), T3 (n = 6), and T4 (n = 15). All patients were treated with radical intent

using a Halcyon V3.1 linear accelerator (Varian Medical Systems, Palo Alto, CA, USA), with prescribed doses ranging from 60 Gy to 70 Gy delivered in 29–35 fractions.

2.2 Image Acquisition and Processing Pipeline

Planning computed tomography (CT) and daily cone-beam computed tomography (CBCT) images were exported from the Eclipse Treatment Planning System (version 15.6; Varian Medical Systems, Palo Alto, CA, USA) in DICOM format, together with the corresponding RTSTRUCT files.
The processing pipeline consisted of the following steps: (1) image reconstruction, (2) tumour volume definition, (3) rigid CT–CBCT registration, (4) longitudinal volume-of-interest (VOI) propagation, and (5) radiomic feature extraction (Fig. 1). All steps were applied consistently across patients and fractions to ensure methodological reproducibility.

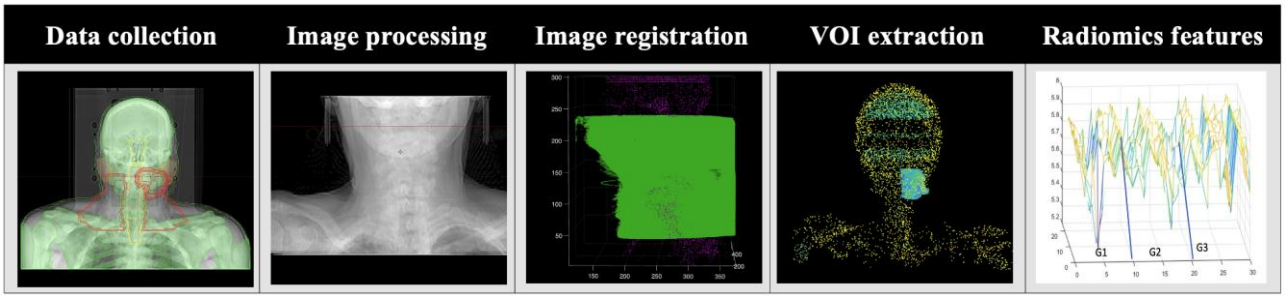


Fig. 1. Overview of the longitudinal CBCT analysis framework

All image preprocessing, registration, and feature extraction procedures were implemented using custom scripts in MATLAB R2025b (MathWorks, Natick, MA, USA; version 24.2.0).

2.3 Image Preprocessing and Volume Reconstruction

DICOM metadata, including voxel spacing and slice thickness, were extracted from all CT and CBCT datasets, and image series were reconstructed into three-dimensional volumes.
Planning CT images were converted to Hounsfield units (HU) using standard DICOM rescaling parameters. In contrast, CBCT intensity values were not considered quantitatively calibrated Hounsfield units because of known variability from scatter, beam hardening, and reconstruction inconsistencies [11]. However, the intensity scale remains approximately aligned with CT attenuation values, enabling the use of consistent relative intensity ranges within a longitudinal, patient-specific analysis framework.
To mitigate these effects, all analyses were performed within a patient-specific longitudinal framework, avoiding direct inter-patient comparison of absolute intensity values. This design enables consistent evaluation of temporal intensity changes while reducing sensitivity to CBCT-specific variability.

2.4 Volume-of-Interest (VOI) Definition and Registration

Tumour volumes of interest were defined using the highest-dose clinical target volume delineated on the planning CT. This ensured consistent inclusion of the primary tumour region receiving the therapeutic dose and provided a stable reference volume across all treatment fractions.
Binary masks were generated from RTSTRUCT files and used to extract tumour regions. To ensure spatial correspondence across longitudinal CBCT acquisitions, VOIs were propagated from planning CT to CBCT images using rigid registration.
Point clouds were generated from VOI masks using the marching cubes algorithm, and rigid alignment between CT- and CBCT-derived point clouds was performed using the iterative closest point (ICP) algorithm implemented in MATLAB. The convergence criterion was set to a maximum of 100 iterations or a mean squared error threshold of 0.001 mm.
Rigid registration was deliberately selected to preserve voxel-level spatial correspondence and avoid interpolation-induced distortions and derived texture features. This approach enables consistent longitudinal sampling of the same anatomical region across time.

2.5 Intensity Thresholding

To focus analysis on tumour-related soft tissue and minimise the influence of irrelevant structures, voxel intensities were restricted to an empirically defined range of −70 to +230 HU on the CT scale. This range was used as a relative threshold within each patient, rather than as an absolute quantitative calibration.

The lower threshold (−70 HU) was chosen to exclude air and low-density regions while retaining water-equivalent and soft tissue intensities associated with oedema and cellular changes. The upper threshold (+230 HU) was based on reported CT attenuation studies for soft tissue (approximately 180 HU) [18], extended to account for CBCT-related intensity variability.

This thresholding strategy was applied consistently across all fractions within each patient and should be interpreted as a soft-tissue-constrained analysis window rather than an absolute HU-based normalisation.

2.6 Radiomic Feature Extraction

Radiomic features were extracted from voxel intensity distributions within longitudinally aligned tumour VOIs on CBCT images for each treatment fraction using custom MATLAB scripts. The extracted features included first-order statistics (mean, median, standard deviation, interquartile range, skewness, kurtosis), as well as entropy (global intensity randomness) and texture descriptors based on the Tamura [19] formulation, including coarseness and strength. Although a broader feature set was initially computed, the analysis focused on entropy, strength, and coarseness, as these features capture complementary aspects of tumour heterogeneity (global randomness, local contrast, and structural scale) and demonstrated the most informative longitudinal behaviour in preliminary analysis.

2.7 Longitudinal Modelling and Statistical Analysis

Longitudinal feature dynamics were analysed using repeated measurements within patients to characterise temporal trajectories and assess differences across tumour differentiation groups (G1–G3). For each feature, temporal behaviour was modelled using linear mixed-effects models implemented in MATLAB (*fitlme* function, Statistics and Machine Learning Toolbox, version 24.2), with fixed effects including treatment fraction, a quadratic fraction term, tumour differentiation group, and their interactions. A patient-specific random intercept was included to account for intra-subject variability across treatment fractions.

Statistical significance of model terms was assessed using analysis of variance (ANOVA), and pairwise comparisons of model coefficients were performed using the *coefTest* function within linear-mixed-effects framework. Non-parametric approaches such as the Kruskal–Wallis test were not applied, as they are limited to comparisons of independent groups and do not allow testing of specific model terms or interactions. In contrast, ANOVA and coefficient-based tests (*coefTest*) within the linear mixed-effects framework enable evaluation of temporal effects and group-dependent differences. A two-sided p-value < 0.05 was considered statistically significant. To characterise nonlinear temporal behaviour, the vertex of the fitted quadratic trajectory was calculated from the estimated linear and quadratic coefficients, corresponding to the treatment fraction at which the feature reached its extremum.

Associations between radiomic features were evaluated using Spearman rank correlation coefficients (r_s) with corresponding 95% confidence intervals (CI). Correlation analysis was performed on patient-level aggregated (median) feature values and served as a complementary assessment of inter-feature relationships. A two-sided p-value of less than 0.05 was considered statistically significant. All statistical analyses were performed using MATLAB R2025b (MathWorks) and IBM SPSS Statistics version 31 (IBM Corp., Armonk, NY, USA).

2.7.1 Entropy

Entropy was used to quantify the degree of randomness in voxel intensity distribution within the aligned tumour VOI and was interpreted as a global measure of intensity heterogeneity. For each treatment fraction, entropy was calculated from normalised histogram probabilities of voxel intensities within the soft-tissue-constrained VOI as follows:

$$entropy = -\sum_{i=1}^{n}(p_i \cdot \log_2(p_i)) \qquad (1)$$

where p_i denotes the normalised histogram probability of density bin *i.* Patient-specific longitudinal entropy trajectories are shown in Fig. 2. Entropy dynamics were analysed using the mixed-effects modelling framework described in section 2.7, including linear and quadratic fraction terms, tumour differentiation group, and their interactions. The turning point of the fitted quadratic entropy trajectory was estimated from the model coefficients to identify the fraction at which the population-level trend reached its maximum.

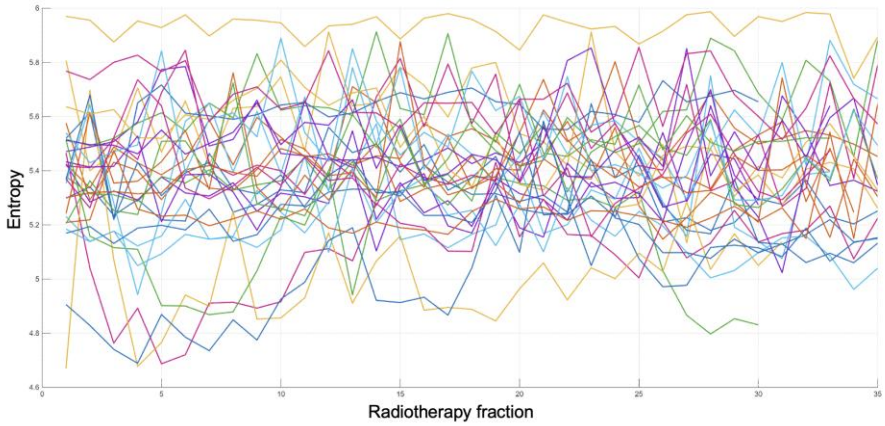


Fig. 2. Longitudinal entropy trajectories in individual patients

To analyse temporal dynamics, a linear mixed-effect model was employed:

$$Entropy_{ij} = \beta_0 + \beta_F Fraction_{ij} + \beta_{F^2} Fraction_{ij}^2 + \beta_G Group_i + \beta_{GF}\left(Group_i \times Fraction_{ij}\right) + \beta_{GF^2}\left(Group_i \times Fraction_{ij}^2\right) + u_i + \varepsilon_i j \quad (2)$$

where $Entropy_{ij}$ denotes the entropy value for patient i at fraction j, β_0 is the intercept, β_G represents the effect of tumour differentiation group, β_F and β_{F^2} denote the linear and quadratic effects of treatment fraction, respectively, β_{GF^2} $_{GF}$ and [illegible] represent the interaction effects between group and the linear and quadratic fraction terms, respectively, u_i is the patient-specific random intercept accounting for inter-patient variability and ε_{ij} is the residual error term.

A quadratic term ($Fraction^2$) was included to account for potential non-linear temporal behaviour of entropy during radiotherapy. The tumour differentiation group (G1, G2, G3) was included as a fixed effect to assess group-level differences in entropy dynamics.

The vertex of the fitted quadratic entropy trajectory, corresponding to the treatment fraction at which entropy reaches its extremum, was calculated as:

$$X = -\beta_F/(2\beta_{F^2}) \quad (3)$$

where β_F and β_{F^2} are the estimated coefficients of the linear and quadratic terms, respectively.

Additionally, interaction terms between treatment fraction and tumour differentiation group were included to evaluate group-specific differences in longitudinal entropy trajectories.

2.7.2 Strength

Strength was used to quantify local intensity contrast within a tumour VOI and characterise fine-scale heterogeneity. Strength was computed using Tamura [19] texture formulation, based on discretised voxel intensities and local grey-level differences:

$$Strength = \frac{\Sigma_i \Sigma_j (p_i + p_j)(i-j)^2}{\Sigma_k s_k} \quad (4)$$

where i *and* j denote discretised grey levels, p_i and p_j are the corresponding intensity probabilities, and s_k represents local intensity differences at voxel position k. Patient-specific longitudinal strength trajectories are shown in Fig. 3. Temporal dynamics of strength were analysed using the same mixed-effects modelling framework, including linear and quadratic fraction terms, tumour differentiation group, and their interactions. The vertex of the fitted quadratic model was calculated to identify the turning point in the population-level strength trajectory.

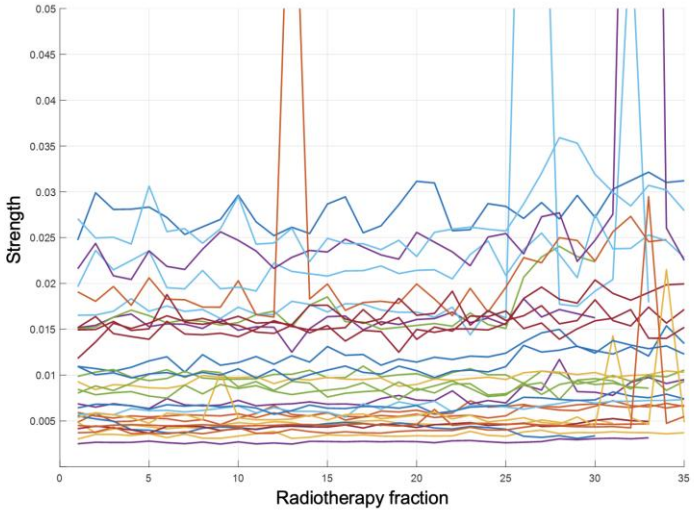


Fig. 3. Longitudinal strength trajectories in individual patients

The quadratic term (*Fraction*^{2}) was included to account for potential non-linear temporal behaviour during radiotherapy. Interaction terms between treatment fraction and tumour differentiation group were additionally included to assess group-specific differences in longitudinal strength trajectories.
The vertex of the fitted quadratic model was calculated to identify potential turning points in strength dynamics, corresponding to extrema in local intensity contrast during treatment.

2.7.3 Coarseness

Coarseness was used to quantify the spatial scale of intensity variation within the tumour VOI and was interpreted as a descriptor of structural organisation. Coarseness was calculated using Tamura [19] formulation, which identifies the dominant local neighbourhood size associated with maximum local intensity variation:

$$Coarseness = \frac{1}{N}\sum_{n=1}^{N} S(n) \qquad (5)$$

Where $S(n)=2^{k^*(n)}$ denotes local structural scale at voxel position n, $k^*(n)$ is the neighbourhood size that maximises local intensity differences, and N denotes the total number of voxels in the tumour VOI. Patient-specific longitudinal coarseness trajectories across radiotherapy fractions are illustrated in Fig. 4. Coarseness dynamics were analysed using the same mixed-effects modelling framework as described in section 2.7 for entropy and strength, enabling evaluation of both overall temporal trends and group-dependent differences in longitudinal structural organisation.

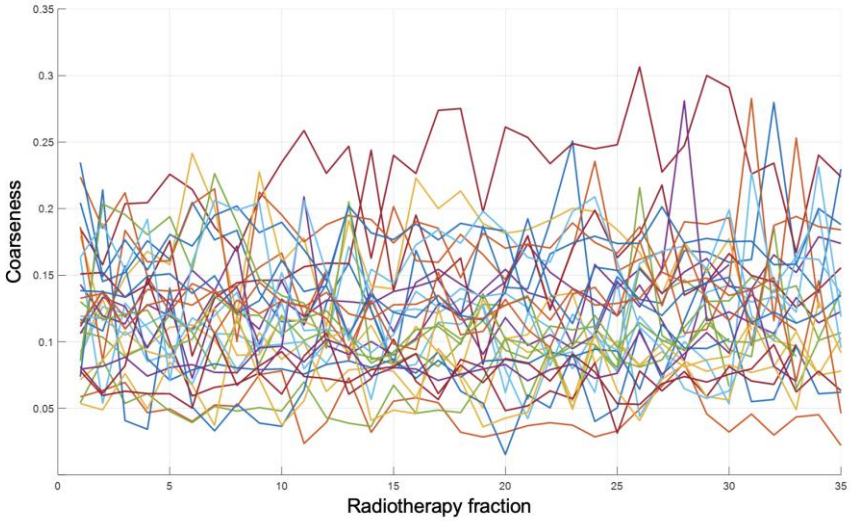


Fig. 4. Longitudinal coarseness trajectories in individual patients

3 Results

Longitudinal analysis of propagated tumour volumes on daily CBCT revealed heterogeneous on-treatment response patterns across the cohort. Three descriptive volume behaviours were observed across patients: progressive volume decrease, relative volumetric stability, and apparent on-treatment volume increase. These patterns varied among differentiation groups, with G1 tumours more frequently showing stable or increasing volume, G2 tumours demonstrating intermediate trajectories, and G3 tumours more often showing stable to modestly regressive patterns (Fig. 5). Because this study was not designed for formal response classification, these observations are reported as descriptive imaging patterns rather than clinical response categories.

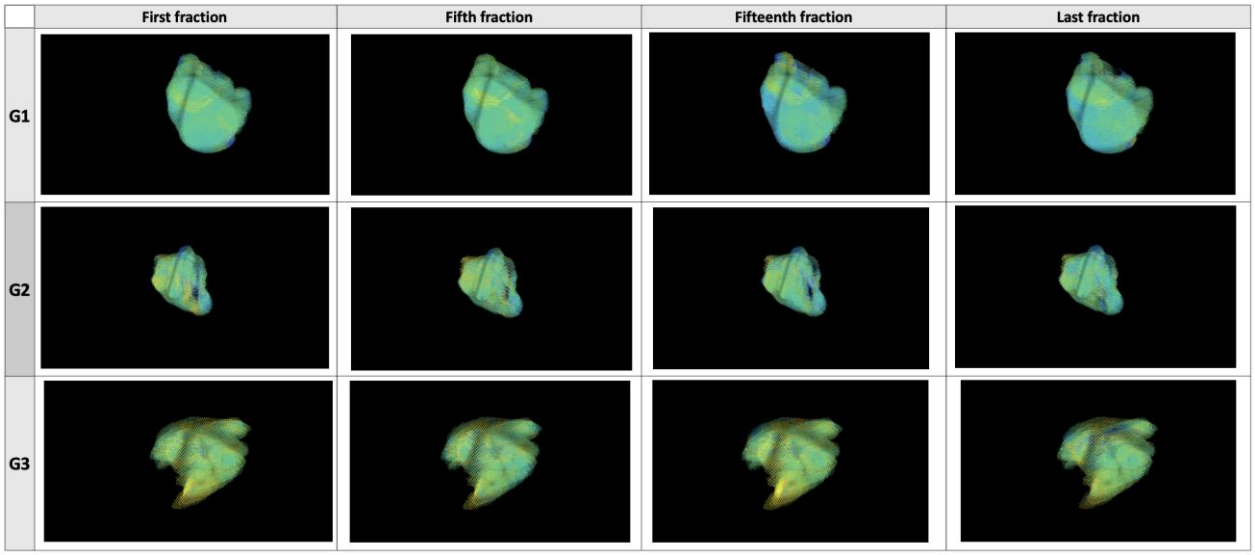


Fig. 5. Representative CBCT-derived tumour volumes across treatment fractions

In addition to volumetric variation, substantial inter-patient heterogeneity was observed in longitudinal texture evolution. At the cohort level, entropy, strength, and coarseness exhibited distinct temporal behaviours, indicating that these features do not contribute equally to the characterisation of treatment-induced structural change. Among the features investigated, coarseness showed the most visually coherent group-level trajectories, whereas entropy displayed the greatest between-patient dispersion.

3.1 Entropy Analysis

The linear mixed-effects model identified a significant temporal dependence of entropy on treatment fraction, with both linear and quadratic terms reaching statistical significance (linear term: $F(1,1015) = 11.30$, $p < 0.001$; quadratic term: $F(1,1015) = 10.97$, $p < 0.001$), consistent with a nonlinear longitudinal trajectory (Fig. 6). No significant main effect of differentiation group was observed in the base model ($F(2,1015) = 1.68$, $p = 0.187$). The fitted population-level trajectory, derived from the fixed effects of the model, showed an inverted U-shaped pattern, with an initial increase followed by a subsequent decrease over the course of treatment. This pattern was supported by a positive linear coefficient ($\beta_F = 0.0062$, $t(1015) = 3.36$, $p < 0.001$) and negative quadratic coefficient ($\beta_{F^2} = -0.000168$, $t(1015) = -3.31$, $p < 0.001$). The estimated vertex of the quadratic fit occurred at approximately 18th fraction (95% CI:16-20), indicating that at this specific fraction entropy reaches its maximum at the population level.

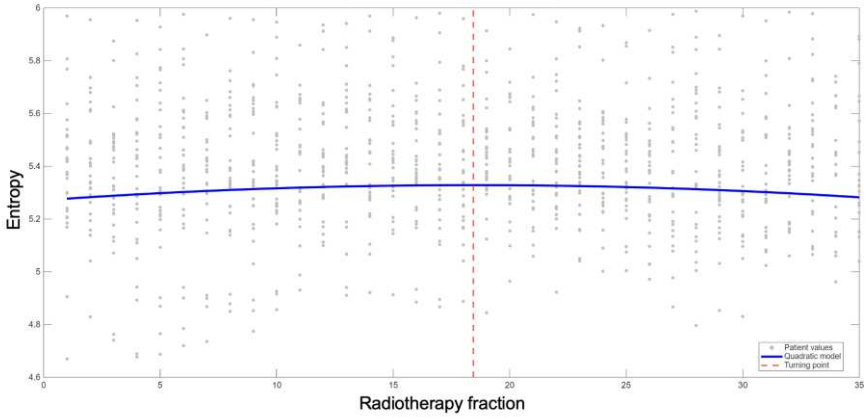


Fig. 6. Population-level entropy trajectory with fitted quadratic model (red dashed line, 18th fraction)

When interaction terms were introduced, a significant interaction was observed between differentiation group and the quadratic treatment term ($F(2,1011) = 3.40$, $p = 0.034$), indicating group-dependent differences in the curvature of the entropy trajectory. In contrast, the interaction between group and the linear treatment term did not reach statistical significance ($F(2,1011) = 2.57$, $p = 0.077$), suggesting that differences between groups are primarily driven by non-linear rather than linear temporal effects. Pairwise coefficient comparisons of the quadratic interaction term showed a significant difference between G2 and G3 ($F(1,1011) = 6.63$, $p = 0.010$), whereas the G1–G2 ($F(1,1011) = 0.72$, $p = 0.396$) and G1–G3 ($F(1,1011) = 2.85$, $p = 0.092$) comparisons were not significant (Fig. 7).

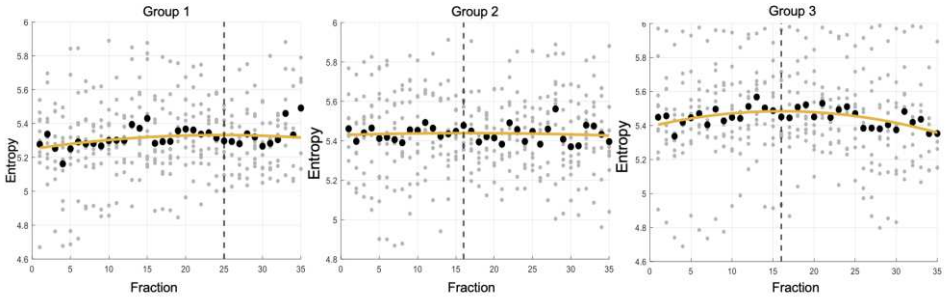


Fig 7. Group-stratified entropy trajectories by tumour differentiation

Group-specific vertex estimates suggested delayed entropy maxima in G1 relative to G2 and G3. The estimated peak occurred between the 24th and 25th fractions for G1, compared with the 16th and 17th fractions for G2 and G3 (Fig. 8). Despite these group-level differences, entropy trajectories showed substantial inter-patient variability, indicating limited stability of this feature for subject-level longitudinal monitoring.

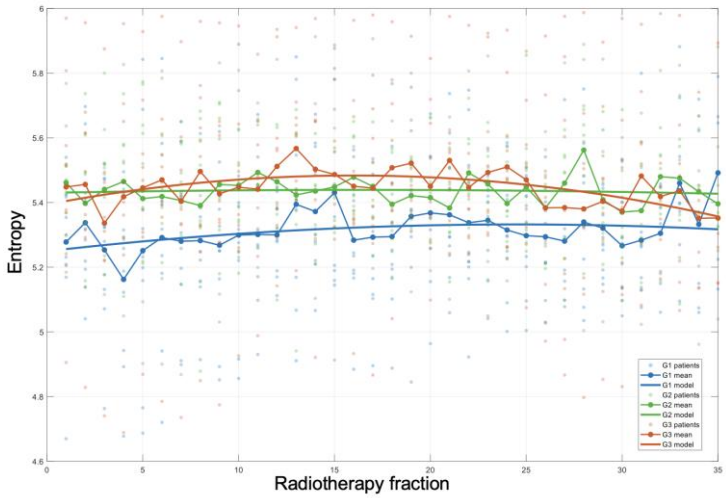


Fig. 8. Group-level entropy with quadratic fits

3.2 Strength Analysis

Strength showed weaker temporal organisation than entropy. In the mixed-effects model without interaction terms, the quadratic effect of treatment fraction was significant (*F(1,1015) = 10.00, p = 0.002*), while the linear term was not significant (*F(1,1015) = 2.82, p = 0.093*), indicating a modest nonlinear trajectory (Fig. 9). The fitted curve was U-shaped, with an estimated minimum at approximately 10th fraction. No significant main effect of differentiation group was observed (*F(2,1011) = 0.82*, *p = 0.439*). Similarly, no significant group-dependent interactions were found for either the linear or quadratic fraction term (*F(2,1011) = 0.228, p = 0.796* and *F(2,1011) = 0.577, p = 0.562,* respectively). These results indicate that the longitudinal behaviour of strength was broadly similar across differentiation groups.

Compared with entropy and coarseness, strength displayed a lower discriminatory capacity at the group level. Although a modest temporal trend was present, the feature remained characterised by considerable between-patient variation and limited evidence of differentiation-dependent structure.

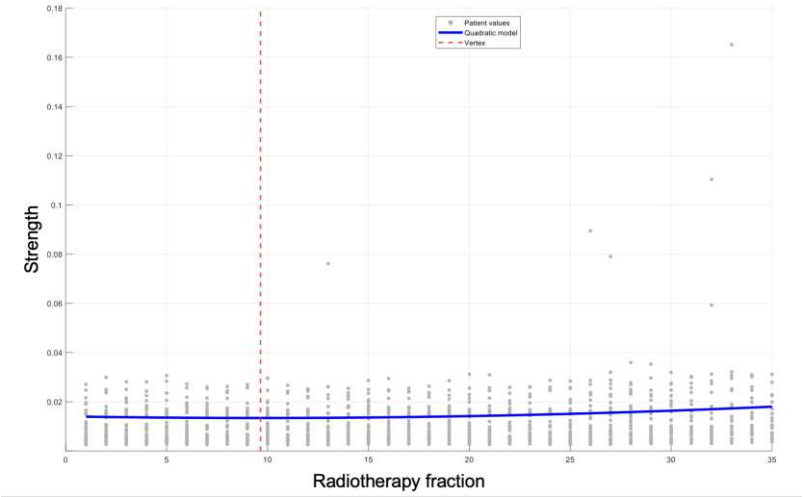


Fig. 9. Population-level strength trajectory with fitted quadratic model

3.2 Coarseness Analysis

In the model without interaction terms, coarseness showed a significant main effect of dependence on tumour differentiation group (*F(1,1015) = 3.10, p = 0.045*), indicating baseline group differences (Fig. 10). Compared to G1, both G2 (β_{G2F^2} *= −0.0366, t(1015) -2.253, p = 0.024*) and G3 (β_{G3F^2} *= −0.0333, t(1015) = -2.047, p = 0.041*) exhibited lower coarseness values. In contrast, neither the linear fraction term (*F(1,1015) = 2.33, p = 0.128*) nor quadratic fraction term (*F(1,1015) = 3.79, p = 0.052*) reached statistical significance in the non-interaction model, although the latter suggested a trend toward nonlinear temporal behaviour.

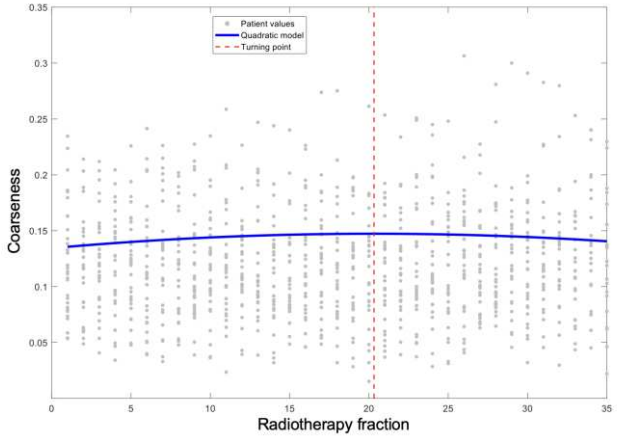


Fig. 10. Populations-level coarseness trajectory with fitted quadratic model

After including interaction terms, the main effect of group was no longer significant (*F(2,1011) = 0.67, p = 0.511*), whereas both the linear and quadratic interactions with differentiation group became significant (linear interaction: *F (2,1011) = 5.99, p = 0.0026;* quadratic interaction: *F(2,1011) = 6.06, p = 0.0024*). These results indicate that differentiation-dependent differences in coarseness are expressed primarily through trajectory shape rather than a simple global offset (Fig. 11).

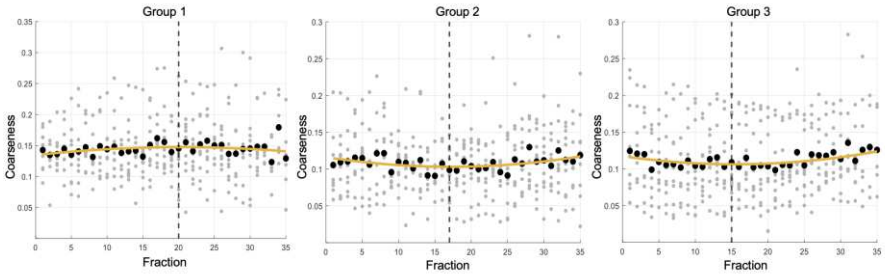


Fig. 11. Group-stratified coarseness trajectories by tumour differentiation

The fitted quadratic coarseness trajectory showed an inverted U-shaped pattern, with a population-level peak at approximately fraction 20. Group-specific vertex estimates indicated progressively earlier turning points from G1 to G3, with peaks at fractions (~20, ~17, and ~16) for G1, G2, and G3, respectively. Pairwise comparisons showed significant differences between G1 and G2 (*F(1,1011) = 9.263, p = 0.0024*) and G1 and G3 (*F(1,1011) = 9.042, p = 0.0027*), whereas no significant difference was observed between G2 and G3 (*F(1,1011) = 0.004, p = 0.953*) (Fig. 12).

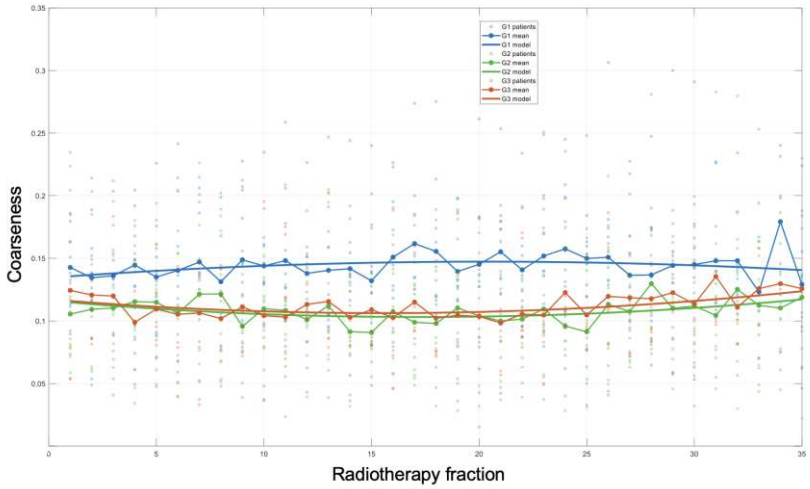


Fig. 12. Group-level coarseness trajectories with quadratic fits

Among the investigated features, coarseness showed the clearest group-dependent temporal structure and the most stable visual trajectory pattern. Compared to entropy and strength, coarseness appeared less affected by high-frequency fluctuation and therefore emerged as the most consistent candidate for longitudinal characterisation of treatment-induced structural change in this cohort.

3.4. Longitudinal association between feature medians

Spearman correlation analysis of aggregated longitudinal feature value was performed to assess inter-feature associations at the cohort level (Table 1) and within tumour differentiation subgroups (Table 2).
In the full cohort, a weak but statistically significant negative association was found between entropy and coarseness (Table I). No significant associations were identified between entropy and strength, or between coarseness and strength. These results suggest partial overlap between information derived from entropy and coarseness, while strength appears to capture a different or less consistent aspect of longitudinal image variation.

Table 1. Spearman correlation between longitudinal median radiomic features for all patients

Feature Pair	Spearman r_s (95% CI)	p-value
Entropy – Coarseness	−0.338 (−0.605, −0.002)	0.047
Entropy – Strength	−0.003 (−0.359, 0.299)	0.849
Coarseness – Strength	−0.047 (−0.370, 0.287)	0.791

At the subgroup level, most associations were not statistically significant (Table 2). In G3, however, entropy was negatively associated with strength, while coarseness showed a positive association with strength. No consistent patterns of inter-feature association were observed across differentiation groups, indicating limited reproducibility of these relationships at the subgroup level.

Table 2. Spearman correlation between longitudinal median radiomic features, stratified by tumour differentiation group

Group	Feature Pair	Spearman r_s (95% CI)	p-value
G1	Entropy – Coarseness	−0.271 (−0.558, 0.075)	0.115
	Entropy – Strength	−0.023 (−0.353, 0.313)	0.896
	Coarseness – Strength	−0.076 (−0.399, 0.265)	0.666
G2	Entropy – Coarseness	−0.039 (−0.368, 0.298)	0.824
	Entropy – Strength	0.088 (−0.254, 0.410)	0.616
	Coarseness – Strength	0.107 (−0.236, 0.426)	0.541
G3	Entropy – Coarseness	−0.278 (−0.564, 0.067)	0.105
	Entropy – Strength	−0.430 (−0.676, −0.097)	0.010
	Coarseness – Strength	0.451 (0.121; 0.691)	0.007

3.5. Summary of feature behaviour

The three analysed radiomic features demonstrated distinct longitudinal profiles. Entropy showed significant but highly variable nonlinear evolution; strength exhibited modest and largely group-independent temporal change; and coarseness showed the most structured and differentiation-dependent trajectories. These findings support a feature-specific interpretation of longitudinal CBCT radiomics, with coarseness providing the strongest signal for robust temporal characterisation in this dataset.

Discussion

The present study demonstrates that longitudinal CBCT-derived radiomic features do not contribute equally to characterising treatment-induced tumour changes during head and neck radiotherapy. Among the features investigated, coarseness exhibited the most stable and structurally coherent temporal behaviour, with lower apparent variability and clearer group-dependent trajectories compared with entropy and strength. In contrast, entropy, although statistically significant at the population level, showed substantial inter-patient variability, while strength demonstrated limited temporal structure and minimal discriminatory capacity. These findings support a feature-specific interpretation of longitudinal CBCT radiomics, in which robustness and temporal stability are critical considerations for biomarker development, consistent with previous observations in radiomics reproducibility studies [20], [21].

In contrast, coarseness demonstrated the most consistent temporal organisation and the strongest differentiation-dependent behaviour. Compared with entropy and strength, coarseness trajectories were characterised by reduced high-frequency, more stable longitudinal trends, and well-defined turning points. The observed nonlinear temporal evolution of entropy, characterised by a mid-treatment peak, is consistent with prior imaging-based studies reporting treatment-induced changes in tumour heterogeneity. Previous CT-based analyses have shown that radiotherapy is associated with measurable reductions in tumour attenuation and structural alterations over time. For example, [22] reported decreases

in CT number within gross tumour volume during treatment, with patient-specific associations to delivered dose, while [23] observed a mean reduction of (52 ± 35) HU in nasopharyngeal tumours, correlated with volumetric regression. Similarly, [24] demonstrated radiation-induced attenuation changes that may be relevant for treatment adaptation. The entropy dynamics observed in the present study may reflect related processes; however, the substantial inter-patient variability indicates that entropy alone may not provide a sufficiently robust descriptor for longitudinal monitoring under CBCT imaging conditions.

Strength exhibited intermediate behaviour, with modest nonlinear temporal variation with no significant group-dependent differences. This suggests that strength primarily reflects local or transient structural variations, which are less consistently associated with differentiation-dependent response patterns. Similar findings have been reported in radiomics studies, indicating that not all extracted features contribute equally to predictive or descriptive performance, and that feature robustness and reproducibility are critical considerations when interpreting radiomic features [20]. In this context, strength may provide complementary information but appears less suitable as a primary longitudinal descriptor under CBCT imaging conditions.

An important contribution of this study is the proposed hierarchical interpretation of longitudinal radiomic features. Within this framework, coarseness functions as a primary descriptor of treatment-induced structural evolution, strength provides secondary information on local contrast variation, and entropy serves as a more variability-sensitive feature reflecting global heterogeneity. This hierarchy is particularly relevant for CBCT-based analysis, where imaging artefacts such as scatter and beam hardening can disproportionately affect features sensitive to intensity fluctuations [11], [13]. Accordingly, the selection of imaging biomarkers should consider not only biological interpretability but also longitudinal stability under realistic imaging conditions.

The temporal ordering observed across features further supports a structured interpretation of treatment-induced changes. In this cohort, strength reached its minimum earlier in treatment, followed by a peak in entropy and a later peak in coarseness. Although this sequence should be interpreted with caution, it suggests a progression from early local contrast reduction to increased global heterogeneity, followed by larger-scale structural reorganisation. Currently, this observation should be considered hypothesis-generating, as it has not been directly validated against histopathological or clinical outcome data. Nevertheless, it provides a potentially useful conceptual framework for future studies investigating the dynamics of tumour response during radiotherapy.

From clinical and methodological perspectives, a key advantage of the proposed framework is its feasibility. CBCT imaging is routinely acquired during image-guided radiotherapy, enabling longitudinal analysis without additional imaging burden. This makes CBCT-based radiomics an attractive approach for monitoring treatment-induced changes in real time. However, the present findings should be interpreted within the limitations of the study. The analysis was performed on a relatively small cohort, with only 10 patients per differentiation group, which limits statistical power and generalisability. In addition, the use of rigid registration ensures spatial consistency but does not account for complex anatomical deformation. Furthermore, CBCT-derived features remain sensitive to acquisition and reconstruction variability despite the use of a within-patient longitudinal framework. Importantly, this study does not establish a predictive or clinically validated biomarker. Rather, it focuses on characterising feature behaviour under longitudinal CBCT conditions. This distinction is critical, as recent work has shown that imaging-derived features do not necessarily improve all prediction tasks. For example, [25] reported that early clinical variables, particularly weight loss, outperformed early CBCT-derived radiomics for prediction of certain treatment-related toxicities. These findings suggest that the utility of longitudinal CBCT radiomics may depend on the specific clinical endpoint considered.

Future work should focus on validating the observed feature behaviour in larger, multi-institutional datasets and assessing the relationship between longitudinal radiomic trajectories and clinical outcomes, including tumour control and treatment toxicity. In addition, integration of imaging features with clinical, dosimetric, and biological variables may further enhance the interpretability and utility of CBCT-based biomarkers. The present study supports the use of longitudinal CBCT radiomics for characterising treatment-induced tumour changes, while highlighting the importance of feature robustness and temporal stability. Rather than treating radiomic features as interchangeable, the results indicate that coarseness, strength, and entropy play distinct roles, with coarseness emerging as the most promising candidate for longitudinal monitoring under routine CBCT imaging conditions.

Conclusion

This study presents a registration-consistent longitudinal CBCT framework for quantifying treatment-induced tumour morphology during head and neck radiotherapy. By integrating baseline-defined volume propagation, rigid point-cloud registration, and mixed-effects modelling of temporal feature dynamics, the approach enables consistent within-patient analysis of voxel-level imaging features across treatment fractions.

The results show that CBCT-derived radiomic features capture dynamic changes in tumour structure during radiotherapy; however, their longitudinal reliability varies considerably. Among the features examined, coarseness displayed the most stable and structurally consistent temporal behaviour, with clearly differentiation-dependent

trajectories. In contrast, entropy exhibited significant but highly variable dynamics, and strength showed limited discriminatory capacity.
These findings support a feature-specific and hierarchical interpretation of longitudinal radiomics, where coarseness may serve as a primary descriptor of treatment-induced structural change, supported by complementary features such as strength, while entropy provides more variability-sensitive information. Importantly, this work highlights that feature robustness and temporal stability are critical considerations for the development of CBCT-based imaging biomarkers.
The proposed framework utilises routinely acquired CBCT data and may facilitate future research in longitudinal treatment monitoring and adaptive radiotherapy. Further validation in larger cohorts and evaluation against clinical outcomes is necessary to establish its clinical utility.

Declarations

Ethics approval and consent to participate

This retrospective study was approved by the Kaunas Regional Biomedical Research Ethics Committee (No. BE-2-144) and conducted in accordance with the principles of the Declaration of Helsinki. The requirement for individual patient consent was waived due to the retrospective nature of the study and the use of fully anonymised data.

Consent for publication

Not applicable.

Availability of data and materials

The datasets generated or analysed during the current study are available from the corresponding author upon reasonable request. Due to patient privacy regulations, individual patient data cannot be made publicly available.

Competing interests

The authors declare that they have no competing interests.

Funding

The work received funding from Lithuanian Research Council, project No P-ITP-25-1.

Authors' contributions

GK: Conceptualisation, methodology, data curation, formal analysis, investigation, writing – original draft. DML: Conceptualisation, methodology, supervision, writing – original draft, writing – review and editing. RCT: Conceptualisation, investigation, data curation, formal analysis, writing – review and editing. RP: Conceptualisation, methodology, investigation, data curation, writing – original draft. VS: Data curation, formal analysis, writing – original draft. RP: Data curation, formal analysis, writing – review and editing. All authors read and approved the final manuscript.

Acknowledgements

The work received funding from Lithuanian Research Council, project No P-ITP-25-1.

References

[1] G. Anderson, M. Ebadi, K. Vo, J. Novak, A. Govindarajan, and A. Amini, “An Updated Review on Head and Neck Cancer Treatment with Radiation Therapy,” *Cancers*, vol. 13, no. 19, p. 4912, Sep. 2021, doi: 10.3390/cancers13194912.
[2] K. Guo, W. Xiao, X. Chen, Z. Zhao, Y. Lin, and G. Chen, “Epidemiological Trends of Head and Neck Cancer: A Population-Based Study,” *BioMed Research International*, vol. 2021, p. e1738932, Jul. 2021, doi: 10.1155/2021/1738932.
[3] Q. Li, Y. Tie, A. Alu, X. Ma, and H. Shi, “Targeted therapy for head and neck cancer: signaling pathways and clinical studies,” *Signal Transduction and Targeted Therapy*, vol. 8, no. 1, Jan. 2023, doi: 10.1038/s41392-022-01297-0.
[4] D. L. Schwartz et al., “Adaptive Radiotherapy for Head-and-Neck Cancer: Initial Clinical Outcomes From a Prospective Trial,” *International Journal of Radiation Oncology*Biology*Physics*, vol. 83, no. 3, pp. 986–993, Jul. 2012, doi: 10.1016/j.ijrobp.2011.08.017.

[5] P. Castadot, J. A. Lee, X. Geets, and V. Grégoire, “Adaptive Radiotherapy of Head and Neck Cancer,” Seminars in Radiation Oncology, vol. 20, no. 2, pp. 84–93, Apr. 2010, doi: 10.1016/j.semradonc.2009.11.002.
[6] N. Buciuman and L. G. Marcu, “Adaptive Radiotherapy in Head and Neck Cancer Using Volumetric Modulated Arc Therapy,” *Journal of Personalized Medicine*, vol. 12, no. 5, p. 668, Apr. 2022, doi: 10.3390/jpm12050668.
[7] W. Luo, Z. Xiu, X. Wang, R. McGarry, and J. Allen, “A Novel Method for Evaluating Early Tumor Response Based on Daily CBCT Images for Lung SBRT,” *Cancers*, vol. 16, no. 1, p. 20, Dec. 2023, doi: 10.3390/cancers16010020.
[8] Z. Peng et al., “Application of radiomics and machine learning in head and neck cancers,” *International Journal of Biological Sciences*, vol. 17, no. 2, pp. 475–486, Jan. 2021, doi: 10.7150/ijbs.55716.
[9] D. C. Marcu, C. Grava, and L. G. Marcu, “Current Role of Delta Radiomics in Head and Neck Oncology,” *International Journal of Molecular Sciences*, vol. 24, no. 3, p. 2214, Jan. 2023, doi: 10.3390/ijms24032214.
[10] S. B. Mali, “Delta Radiomics — Potential Role in Head Neck Cancer,” *Oral Oncology Reports*, p. 100676, Oct. 2024, doi: 10.1016/j.oor.2024.100676.
[11] E. Pfaehler et al., “Repeatability of ^{18} F-FDG PET radiomic features: A phantom study to explore sensitivity to image reconstruction settings, noise, and delineation method,” *Medical Physics,* vol. 46, no. 2, pp. 665–678, Feb. 2019, doi: 10.1002/mp.13322.
[12] C. Guezennec et al., “Inter-observer and segmentation method variability of textural analysis in pre-therapeutic FDG PET/CT in head and neck cancer,” *PLOS ONE*, vol. 14, no. 3, p. e0214299, Mar. 2019, doi: 10.1371/journal.pone.0214299.
[13] M. L. Welch et al., “Vulnerabilities of radiomic signature development: The need for safeguards,” *Radiotherapy and Oncology*, vol. 130, pp. 2–9, Jan. 2019, doi: 10.1016/j.radonc.2018.10.027.
[14] R. T. H. Leijenaar et al., “The effect of SUV discretization in quantitative FDG-PET Radiomics: the need for standardized methodology in tumor texture analysis,” *Scientific Reports*, vol. 5, no. 1, Aug. 2015, doi: 10.1038/srep11075.
[15] C.-C. Liu and J. Qi, “Higher SNR PET image prediction using a deep learning model and MRI image,” *Physics in Medicine and Biology*, vol. 64, no. 11, p. 115004, May 2019, doi: 10.1088/1361-6560/ab0dc0.
[16] R. M. Martens et al., “Adherence to pretreatment and intratreatment imaging of head and neck squamous cell carcinoma patients undergoing (chemo) radiotherapy in a research setting,” *Clinical Imaging*, vol. 69, pp. 82–90, Jan. 2021, doi: 10.1016/j.clinimag.2020.06.047.
[17] J. Wang, J. E. Moon, X. Guo, J. Yu, J. Yi, and S. H. Bae, “The Current Position of Postoperative Radiotherapy for Salivary Gland Cancer: A Systematic Review and Meta-Analysis,” *Cancers*, vol. 16, no. 13, p. 2375, Jun. 2024, doi: 10.3390/cancers16132375.
[18] M. Bogowicz et al., “Computed Tomography Radiomics Predicts HPV Status and Local Tumor Control After Definitive Radiochemotherapy in Head and Neck Squamous Cell Carcinoma,” *International Journal of Radiation Oncology*Biology*Physics*, vol. 99, no. 4, pp. 921–928, Nov. 2017, doi: 10.1016/j.ijrobp.2017.06.002.
[19] H. Tamura, S. Mori, and T. Yamawaki, “Textural Features Corresponding to Visual Perception,” *IEEE Transactions on Systems, Man, and Cybernetics*, vol. 8, no. 6, pp. 460–473, 1978, doi: 10.1109/tsmc.1978.4309999.
[20] W. Zhang, Y. Guo, and Q. Jin, “Radiomics and Its Feature Selection: A Review,” *Symmetry*, vol. 15, no. 10, p. 1834, Oct. 2023, doi: 10.3390/sym15101834.
[21] H. E. Morgan et al., “Exploratory ensemble interpretable model for predicting local failure in head and neck cancer: the additive benefit of CT and intra-treatment cone-beam computed tomography features,” *Quantitative Imaging in Medicine and Surgery*, vol. 11, no. 12, pp. 4781–4796, Dec. 2021, doi: 10.21037/qims-21-274.
[22] M. Feng et al., “Computed tomography number changes observed during computed tomography-guided radiation therapy for head and neck cancer,” *International Journal of Radiation Oncology, Biology, Physics*, vol. 91, no. 5, pp. 1041–1047, Jan. 2015, doi: 10.1016/j.ijrobp.2014.12.057.
[23] S. Xu et al., “Radiation-induced CT number changes in GTV and parotid glands during the course of radiation therapy for nasopharyngeal cancer,” *British Journal of Radiology*, vol. 89, no. 1062, Apr. 2016, doi: 10.1259/bjr.20140819.
[24] M. S. Athiyamaan, A. G. Hasib, C. H. Sridhar, and P. Sudhir, “Radiation-induced changes in volume and CT number of gross tumour volume and parotid glands during the course of IMRT for head and neck cancers,” *Oncology in Clinical Practice*, vol. 13, no. 2, pp. 39–45, 2017, doi: 10.5603/OCP.2017.0007.
[25] C. Bang et al., “Dynamic prediction of Radiotherapy toxicities in Head and neck cancer using clinical and imaging data,” *Radiotherapy and Oncology*, vol. 214, p. 111312, Nov. 2025, doi: 10.1016/j.radonc.2025.111312.